THE FORMATION OF CONCENTRIC VORTICITY STRUCTURES IN TYPHOONS

H.-C. Kuo*

Department of Atmospheric Sciences

National Taiwan University, Taipei, Taiwan

L.-Y. Lin

National Science and Technology Center for Disaster Reduction, Taiwan

C.-P. Chang and R. T. Williams

Department of Meteorology

Naval Postgraduate School, Monterey, CA. 93943

Submitted to JAS

December 12 2003

Revised April 28 2004

∗*Corresponding author address*: H.-C. Kuo, Department of Atmospheric Sciences, National Taiwan University, Taipei, Taiwan. E-mail: kuo@lanczos.as.ntu.edu.tw

Abstract

An important issue in the formation of concentric eyewalls in a tropical cyclone is the development of a symmetric structure from asymmetric convection. We propose, with the aid of a nondivergent barotropic model, that concentric vorticity structures result from the interaction between a small and strong inner vortex (the tropical cyclone core) and neighboring weak vortices (the vorticity induced by the moist convection outside the central vortex of a tropical cyclone). The results highlight the pivotal role of the vorticity strength of the inner core vortex in maintaining itself, and in stretching, organizing and stabilizing the outer vorticity field. Specifically, the core vortex induces a differential rotation across the large and weak vortex to strain out the latter into a vorticity band surrounding the former. The straining out of a large, weak vortex into a concentric vorticity band can also result in the contraction of the outer tangential wind maximum. The stability of the outer band is related to the Fjørtoft sufficient condition for stability because the strong inner vortex can cause the wind at the inner edge to be stronger than the outer edge, which allows the vorticity band and therefore the concentric structure to be sustained. Moreover, the inner vortex must possess high vorticity not only to be maintained against any deformation field induced by the outer vortices but also to maintain a smaller enstrophy cascade and to resist the merger process into a monopole. The negative vorticity anomaly in the moat serves as a "shield" or a barrier to the further inward mixing the outer vorticity field. Our binary vortex experiments suggest that the formation of a concentric vorticity structure requires: 1) a very strong core vortex with a vorticity at least six times stronger than the neighboring vortices, 2) a large neighboring vorticity area that is larger than the core vortex, and 3) a separation distance between the neighboring vorticity field and the core vortex that is within three to four times the core vortex radius.

1. Introduction

Aircraft observations (e.g., Willoughby et al. 1982, Black and Willoughby 1992, hereafter BW92) show that intense tropical cyclones often exhibit concentric eyewall patterns in their radar reflectivity. In this pattern deep convection within the inner, or primary, eyewall is surrounded by a nearly echo-free moat, which in turn is surrounded by a partial or complete ring of deep convection. Both convective regions typically contain well-defined local wind maxima. The primary wind maximum is associated with the inner core vortex, while the secondary wind maximum is usually associated with enhanced vorticity field embedded in the outer rainband. An example of the concentric eyewalls in Hurricane Gilbert (1988) is given in detail by Willoughby et al. (1989) and BW92. Approximately twelve hours after reaching its minimum sea level pressure of 888 hPa, the lowest recorded so far in the Atlantic basin (Willoughby et al. 1989), Hurricane Gilbert displayed concentric eyewalls. BW92 estimated the radius to be between 8 - 20 km for the inner eyewall and 55 - 100 km for the outer eyewall. Between the two eyewalls, an echo-free gap (or moat) of about 35 km exists where the vorticity is low. Aircraft radial observations also showed the contraction of the outer tangential wind maximum from a distance of 90 km from the storm center to 60 km in approximately twelve hours (e.g. Fig. 7, BW92). Moreover, the core vortex intensity remained approximately the same during the contraction of the outer tangential wind maximum.

Shapiro and Willoughby (1982) and Schubert and Hack (1982) used a simple symmetric model of balanced vortex response to specified heating to propose that heating-vorticity interaction can lead to convective-ring contraction. Their mechanisms involved both the specified diabatic heating and the inertial stability structure. If the ring contains active convective heating, the most rapid increase in windspeed lies on the inward side of the wind maximum and the ring may contract

with time. However, the formation of a concentric eyewall was often observed to start from the organization of asymmetric convection outside the primary eyewall into a band that encircled the eyewalls (e.g. Fig. 3 of BW92). It is not yet clear how the symmetric models may be extended to explain the formation of concentric eyewalls from asymmetric convection. Montgomery and Kallenbach (1997) proposed that the concentric eyewalls might be the result of radially propagating linear vortex Rossby waves and the presence of a critical radius in the tropical cyclone. The radially varying vorticity assumes the role of the meridional gradient of the Coriolis parameter. Unlike the planetary Rossby waves that can propagate over large meridional distances, the vortex Rossby waves are more confined to the radius of maximum winds in the tropical cyclone and therefore their role in the contraction of outer bands from a distance of the order 100 km from the storm center may be limited. Kossin et al. (2000) investigated the dynamic stability of concentric vorticity structures in tropical cyclones with a nondivergent barotropic model. Their study shed light on the interactions between a tropical cyclone's primary eyewall and a secondary ring of enhanced vorticity, but the question of the formation of concentric vorticity structures was not discussed. Recently, Nong and Emanuel (2003) have examined the dynamics of axisymmetric concentric eyewall cycles in the context of axisymmetric models. Their study indicates that the secondary eyewalls may result from a finite-amplitude WISHE instability, triggered by external forcings. Asymmetric dynamics processes that are intrinsic to the hurricane vortex are not included in their axisymmetric model.

In this paper we show that the organization of the asymmetric convection into a symmetric concentric eyewall can be accomplished through a binary vortex interaction between a small and strong inner vortex (the tropical cyclone core) and neighboring weak vortices (the vorticity induced by the moist convection outside the

central vortex). Our model is an extension of those of Dritschel and Waugh (1992) and Dritschel (1995), who described the general interaction of two barotropic vortices with equal vorticity but different sizes. They conducted experiments on the f-plane by varying the ratio of the vortex radii and the distance between the edges of the vortices normalized by the radius of the larger vortex. The resulting structures can be classified into elastic interaction, merger, and straining-out regimes. In the complete straining out regime, a thin region of filamented vorticity bands surrounding the central vortex with no incorporation into the central vortex appeared to resemble a concentric vorticity structure. However, the outer bands, which result from the smaller vortex, are much too thin to be identified with that observed in the outer eyewall of a tropical cyclones. In radar observations of Typhoon Lekima of 2001 (Fig 1), we noticed a huge area of convection outside the core vortex that wraps around the inner eyewall to form the concentric eyewalls in a time scale of 12 hours. A similar example may be found of Figs. 2–9 in Hoose and Colón (1970). In these cases the vorticity in the large area outside the core appear to be much weaker than that in the small core area, a situation that was not included in Dritschel and Waugh's study.

In this study a nonlinear barotropic model is used to extend Dritschel and Waugh's (1992) and Dritschel's (1995) study by adding vorticity ratio as a third external parameter, in addition to the radii ratio and the normalized distance between the two vortices. It will be shown that considering this difference of the vorticity of the two vortices is crucial in the formation of concentric vorticity structures. Namely, one way to produce a halo of enhanced vorticity around an intense vortex is through a binary interaction in which the large, weak vortex is completely strained out. It will be shown that this mode of interaction is most likely to occur when the peak vorticity in the small, strong vortex is at least six times that of the

large, weak vortex. Section 2 describes the solution method and the model parameters. The numerical results are presented in section 3, and the concluding remarks are given in section 4.

2. Model and initial conditions

The basic dynamics considered is two-dimensional nondivergent barotropic with ordinary diffusion, i.e., $D\zeta/Dt = \nu\nabla^2\zeta$, where $D/Dt = \partial/\partial t + u(\partial/\partial x) + v(\partial/\partial y)$. Expressing the velocity components in terms of the streamfunction by $u = -\partial\psi/\partial y$ and $v = \partial\psi/\partial x$, we can write the nondivergent barotropic model as

$$\frac{\partial\zeta}{\partial t} + \frac{\partial(\psi,\zeta)}{\partial(x,y)} = \nu\nabla^2\zeta, \tag{1}$$

where

$$\zeta = \nabla^2\psi \tag{2}$$

is the invertibility principle and $\partial(\ ,\ )/\partial(x,y)$ is the Jacobian operator. The diffusion term on the right hand side of (1) controls the spectral blocking associated with the enstrophy cascade to higher wave numbers. Similar to Prieto et al. (2001) and Kossin et al. (2000), we have avoided the use of hyperviscosity (higher iterations of the Laplacian operator on the right hand side of (1)) because of the unrealistic oscillations it can cause in the vorticity field. Three integral properties that we shall monitor during our numerical simulations are the energy $E = \iint \frac{1}{2}\nabla\psi\cdot\nabla\psi\,dxdy$, the enstrophy $Z = \iint \frac{1}{2}\zeta^2\,dxdy$, and the palinstrophy $P = \iint \frac{1}{2}\nabla\zeta\cdot\nabla\zeta\,dxdy$, a measure of the overall vorticity gradient in the domain. As can be shown from (1) and (2), these three integral properties are related by

$$\frac{dE}{dt} = -2\nu Z, \tag{3}$$

$$\frac{dZ}{dt} = -2\nu P. \tag{4}$$

We perform calculations on the doubly periodic f-plane. The discretization of the model is based on the Fourier pseudospectral method, with 512×512 equally spaced collocation points on a 200 km $\times$ 200 km domain for the binary vortex interaction experiments and a 600 km $\times$ 600 km domain for the Lekima experiment.

The code was run with a dealiased calculation of quadratic nonlinear terms with 170×170 Fourier modes. Time differencing was via the fourth-order Runge-Kutta method with a 6 second time step. The diffusion coefficient, unless otherwise specified, was chosen to be $\nu = 6.5$ m^2 s^{-1}. For the 200 km $\times$ 200 km domain this value of ν gives a e^{-1} damping time of 45 minutes for all modes having total wave number 170, and a damping time of 3 hours for modes having total wave number 85. Some of the experiments were performed at doubled the domain size. Results were found not to be sensitive to the domain size.

We consider initial conditions consisting of J Rankine-like vortex patches [1], i.e.,

$$\zeta(x, y, 0) = \sum_{j=1}^{J} \zeta_j P(r_j), \tag{5}$$

where ζ_j is the vorticity in the jth vortex patch, $r_j = \left[(x - x_j)^2 + (y - y_j)^2\right]^{\frac{1}{2}} / R_j$ is a nondimensional radial coordinate, x_j, y_j are the center coordinates, R_j is the

[1] The Rankine vortices are with zero vorticity gradient and rapid decrease of angular velocity with radius outside the core. DeMaria and Chan (1984) argued that mergers in binary vortex interaction can also occur due to vortex propagation on the outer vorticity gradients associated with each vortex. The interaction of the tangential wind field with the outer vorticity field of the opposite vortex adds a component to the motion which can cause the separation distance to either decrease or increase, depending on the direction of the vorticity gradient. Thus, the extended vorticity gradient in a more realistic vortex should make merger more likely (or less likely) than with the Rankine structure. Moreover, the slower decrease of angular velocity associated with the extended vorticity gradient should slow the filamentation process.

radius of the jth vortex patch, and

$$P(r_j) = \begin{cases} 1 - \exp[-\frac{30}{r_j}\exp(\frac{1}{r_j - 1})], & \text{if } r_j < 1, \\ 0, & \text{otherwise} \end{cases} \tag{6}$$

is an analytical approximation to the unit step function, which has been introduced to reduce the Gibbs phenomenon in the initial condition. Our experiments include both binary vortex interactions (i.e., $J = 2$) and multiple vortex interactions. For the large, weak vortex we assume $\zeta_2 = 3 \times 10^{-3}$ s^{-1} and for the small, intense vortex we assume $R_1 = 10$ km. For the binary vortex interaction experiments with d as the distance between the vortex centers, the binary vortices are specified by choosing numerical values for the dimensionless gap

$$\frac{\triangle}{R_1} = \frac{d - (R_1 + R_2)}{R_1}, \tag{7}$$

the vorticity strength ratio

$$\gamma = \frac{\zeta_1}{\zeta_2}, \tag{8}$$

and the vortex radius ratio

$$r = \frac{R_1}{R_2}. \tag{9}$$

Figure 2 depicts the parameters for the binary vortex experiments. The parameter ranges studied in this paper are $0 \leq \triangle/R_1 \leq 4$, $1 \leq \gamma \leq 10$, and $1/4 \leq r \leq 1$.

3. Numerical results

a. binary vortex interaction

We consider the binary vortex interaction similar to Dritschel and Waugh (1992) except that we have the vortex strength ratio as an additional control parameter. Specifically, we use a small and strong vortex to represent the tropical cyclone core vortex and a large and a weaker vortex to represent the relatively weak vorticity induced by the moist convection outside the central vortex of a tropical cyclone. The idealization stems from the Lekima observation that the eye core was surrounded by a huge area of convection before the formation of concentric eyewalls. Figure 3 shows the sensitivity of the vorticity field with respect to the vorticity strength ratio (γ) at hour 0, 3, 6, and 12 with the dimensionless gap $\triangle/R_1 = 1$, and the vortex radius ratio $r = 1/3$. It is clear from Fig. 3 that the two vortices undergo a behavior ranging from merger ($\gamma = 1$ and $\gamma = 3$), to tripole formation ($\gamma = 5$), to concentric vorticity structure with a moat ($\gamma = 6$). The tripole is an elliptical inner vortex and two distinctive minima in the moat. The last regime explains the results of Ritchie and Holland (1993) who included the interaction between a small, strong vortex and a large, weak vortex in one of their experiments. They did not produce a concentric vorticity structure apparently because their vorticity strength ratio did not exceed 3. Figure 3 suggests that the core vorticity of the small vortex is crucial in the formation of concentric vorticity structure. In the case of concentric vorticity formation ($\gamma = 6$), we observe a straining out of the weak vortex into a thin band that spirals into and surrounds the strong core vortex at hour 3, with subsequent development of concentric vorticity structure and tightly wound spiral bands. This suggests that there are active merger dynamics occurring from hour 3 until the more stable and coherent concentric vorticity structure is reached at hour 12. Kossin et

al. (2000) investigated the dynamical stability of concentric vorticity structures in tropical cyclones with a nondivergent barotropic model. Two types of instabilities were identified: 1) instability across the outer ring of enhanced vorticity, and 2) instability across the moat. Type 1 instability occurs when the outer vorticity band is sufficiently narrow and the inner vortex is sufficiently weak that it does not induce enough differential rotation across the outer vorticity to stabilize it. Type 2 instability occurs when the radial extent of the moat is narrow so that barotropic instability may result. In the case of the Type 2 instablity, Kossin et al. (2000) found that the moat and vortex evolve into a nearly steady tripole structure. The formation of the tripole vortex in the $\gamma = 5$ case apparently involves the straining out of the larger, weaker vortex into a finite width band surrounding the smaller, stronger vortex, with a subsequent type 2 instability of wavenumber 2 across the moat. Two examples of elliptical eyes that resemble the tripole vortex structure were recently reported by Kuo et al. (1999) for the case of Typhon Herb (1996), and by Reasor et al. (2000) for the case of Hurricane Olivia (1994). On the other hand, neither type 1 nor type 2 instabilities (Kossin et al. 2000) are favored for $\gamma = 6$ and $\triangle/R_1 = 1$. Even though the change of sign of vorticity gradient across the outer band satisfies the Rayleigh necessary condition for barotropic stability, the band is stabilized by the Fjørtoft sufficient condition for stability. Namely, the strong inner vortex causes the wind to be stronger at the inner edge than the outer edge, allowing the vorticity band and therefore the concentric structure to be sustained. A similar mechanism is discussed by Dritschel (1989) and Polvani and Plumb (1992), who showed how thin filaments can be stabilized by the flow field of the main vortex. They argued that the filament is linearly stable and appears circular in the presence of sufficiently strong "adverse shear". The adverse shear is

an externally controlled parameter with the opposite sense as that produced by the filament's vorticity alone.

Figure 4 is similar to Fig. 3 and shows the sensitivity of the vorticity field to the dimensionless gap $\triangle/R_1$ with the vortex size ratio $r = 1/3$ and the vorticity ratio $\gamma = 5$. Figure 4 suggests that a moderate dimensionless gap (e.g., $\triangle/R_1 = 2$) is favored for the formation of a concentric vorticity structure. A weaker vortex that is too far away leads to an elastic interaction, while a weaker vortex that is too close will lead to the formation of a tripole vortex. Complete merger occurs when $\gamma = 5$ and the gap vanishes. The simulation is in general agreement with the stability analysis by Kossin et al. (2000). In their Fig. A1, the wavenumber 2 instability (which leads to the formation of a tripole vortex) has a sharp boundary for the r_1/r_2 parameter, such that the instability vanishes at $r_1/r_2 \leq 0.55$. The corresponding parameter of their r_1/r_2 is related to our dimensionless gap $\triangle/R_1 = 1/(r_1/r_2) - 1$. Thus, a larger dimensionless gap of 2 (and thus a larger resultant moat size) will not have type 2 instability, so that the concentric vorticity structure can be maintained.

Figure 5 is similar to Fig. 3 and shows the sensitivity of the vorticity field to the vortex size ratio r with the dimensionless gap $\triangle/R_1 = 1$, and the vorticity ratio $\gamma = 5$. The concentric vorticity structure forms at $r = 1/2$ and tripole vortices form with size ratios of 1/3 and 1/4.

Figure 6 is similar to Fig. 5 except that $\triangle/R_1 = 0$ and $\gamma = 10$. For all but the $r = 1$ case, a concentric vorticity structure forms when the core vortex is 10 times stronger. Other tests with $\gamma = 10$ and $\triangle/R_1$ up to 3 or 4 also yield concentric vorticity structures in every case in which the r parameter is smaller than unity (the weaker vortex is larger in size than the core vortex.) The formation of the moat region at $\triangle/R_1 = 0$ and $\gamma = 10$ occurs through the advection of the negative vorticity anomaly from the background vortex-free-region. The strong differential

rotation outside the radius of maximum wind of the core vortex may also contribute to the formation and maintenance of the moat. Rozoff et al. (2003) have examined the rapid filamentation zones in intense tropical cyclone. They argued that the strain-dominated flow region outside the radius of maximum wind of the core vortex can contribute significantly to the moat dynamics.

Figure 7 shows the sensitivity of the vorticity field in the binary vortex experiments with respect to the diffusivity ν at hour 0, 6, 12, and 36 when $\gamma = 5$, $r = 1/3$, and $\triangle/R_1 = 2.5$. Figure 7 suggests that concentric vorticity structures change to tripole structures at hour 12 if we employ a diffusion which is ten to thirty times larger than $\nu = 6.5$ m^2 s^{-1}. The tripole structure in the highest diffusion case ($\nu = 97.5$ m^2 s^{-1}) becomes a monopole structure at hour 36, while the $\nu = 32.5$ m^2 s^{-1} case retains a tripole structure. The relatively small vorticity in the moat prohibits radial movement due to the dynamics of inertial stability. The negative vorticity anomaly in the moat serves as a "shield" to impose a barrier to the inward mixing of the outer vorticity field. On the other hand, tripole structures may result from the reduction of the moat size due to a larger ν in the period between hours 6 and 12. The wave number 2 growth from type 2 instability, as analyzed by Kossin et al. (2000), then sets the stage for tripole formation.

The time dependence of kinetic energy, enstrophy, and palinstrophy for the experiments in Fig. 7 are shown in Fig. 8. The near conservation of the kinetic energy, the damping of the enstrophy field, and the initial increase and the eventual decrease of the palinstrophy field all possess the characteristics of two dimensional turbulence. The larger values of ν leading to the tripole and monopole cases are associated with a more active enstrophy cascade, as seen in Fig. 8. The small humps in the palinstrophy around hour 34 for the $\nu = 6.5$ m^2 s^{-1} and $\nu = 3.25$ m^2 s^{-1} cases are due to the straining out of a small satellite vortex. The formation of a

tripole instead of a concentric vortex, and the formation of a monopole with the largest ν, appears to be related to selective decay of enstrophy versus kinetic energy and the resulting merger process in two-dimensional turbulence (Batchelor 1969). In the case of a nearly inviscid fluid (where ν is very small), the vorticity contours can pack close together before diffusion is effective. The closely packed contours increase $|\nabla\zeta|$, and hence the palinstrophy as shown in Fig. 8. Even when ν is small, the $-2\nu P$ term on the right hand side of (4) may not be small due to the increase of palinstrophy. We then have a significant enstrophy cascade. With significant enstrophy cascade (thus a smaller enstrophy later), the right hand side of kinetic energy equation (3) is small and the kinetic energy is nearly conserved. This is the phenomenon of the *selective decay*, i.e., the enstrophy is selectively decayed over kinetic energy, in the two-dimensional turbulence (Cushman-Roisin 1994). In the presence of strong rotation, the wind field is nearly geostrophic, so that

$$u \sim \frac{\triangle p}{l}, \tag{10}$$

the kinetic energy is

$$E \sim u^2 \sim \frac{\triangle p^2}{l^2}, \tag{11}$$

and the enstrophy is

$$Z \sim (u/l)^2 \sim \frac{\triangle p^2}{l^4}, \tag{12}$$

where $\triangle p$ is the pressure perturbation and l is the vortex scale. The near conservation of energy, as illustrated in Fig. 8, according to (11), requires that $\triangle p/l$ remains approximately constant. The cascade of enstrophy according to (12), along with the conservation of kinetic energy, imply a steady increase of l, with a proportional increase in $\triangle p$. Thus, the vortices become, on the average, larger, stronger, and fewer. There is thus a natural tendency toward larger structures with successive eddy mergers. With every merger, energy is consolidated into larger structures

with concomitant enstrophy losses. Thus, the merger processes and the formation of monopole in a nearly inviscid fluid can be more significant with a larger ν. To conserve angular momentum and/or kinetic energy during the merger process, the inward merger of the vorticity field toward the core vortex must be accompanied also by some outward vorticity redistribution (Schubert et al. 1999). The outward redistribution can be seen in the form of filaments that orbit the core vortex. On the other hand, coherent vorticity structures such as the concentric vortex and the tripole vortex can prolong the merger process. The merger processes can be seen in our model results with which noticeable spiral bands at hour 3 and 6 but not at hour 12 when the concentric vorticity and tripole structures are formed. The results suggest that there are active merger dynamics occurring at hours 3 and 6, after which a more stable and coherent concentric vorticity structure is reached at hour 12. We observed in Fig. 7 that the concentric vortex patterns change to tripole patterns when ν is increased. The increase of ν, the increase of enstrophy cascade or the increase of the merger process presumably can reduce the moat size and lead to the wave number 2 instability. The increase of ν can occur when tropical cyclones make landfall and the friction from the boundary layer increases. Willoughby (1990) pointed out that the outer eyewall may not survive if the storm is close to land. The collapse of the concentric eyewalls, however, may not be adequately modeled with only advective dynamics.

Figure 9 shows the results of experiments with the same maximum wind in the core vortices but with variations in the core vortex radius and the maximum vorticity. Specifically, we considered the core vortices that possess the vorticity and radius of (1.8×10^{-2} s^{-1}, 10 km) and (0.9×10^{-2} s^{-1}, 20 km) respectively. The pair of core vortices considered induce the same deformation field or differential rotation in the region outside the radius of maximum wind. The dimensionless

gap is 1 in the experiments. The outer vortices considered have the radius of 30 km and 40 km respectively. The γ and r parameters in the first two experiments are (6, 1/3) and (3, 2/3) respectively. They indicate that a similar concentric vorticity structure formed except that the double-size core vortex case possesses a thinner outer band. The thinner band is a result of more active merger of outer vorticity into the core as well as a larger perimeter surrounding the core. The γ and r parameters in the bottom half of Fig. 9 are (6, 1/4) and (3, 2/4) respectively. We observe that the smaller stronger vortex simulation results in a tripole while the corresponding case results in a monopole. In these experiments with the same maximum tangential wind, the larger, weaker (in terms of vorticity) inner vortices undergo more distortion and more active merger with the neighboring vortices. The experiments, along with the experiments shown in Figs. 3, 5 and 6, suggest that the inner vortex has to be strong not only to maintain itself against any deformation field due to outer vortices, but also to possess smaller enstrophy cascade and to resist the merger process into a monopole. The resistance of the stronger inner vortex to deformation and merger agrees with 2D turbulence experiments (McWilliams 1984) and with atmospheric observations and theories (Bowman 1996, McIntyre 1989), that high vorticity gradients protect vortex cores from violent interaction. When the vorticity gradient is sharp, any radial flow will quickly produce a large anomaly and quickly propagate away by the vortex Rossby wave along the edge before any further penetration has occurred. An equivalent explanation is that a high vorticity core exerts a high inertial stability and prevents radial penetration of the outside fluid into the core. Figure 9 also supports the notion that the vorticity strength ratio, not the maximum tangential wind ratio, is the more useful experimental parameter.

Figure 10 gives the interaction regimes for binary vortices calculated as a function of the dimensionless gap $\triangle/R_1$ and the vorticity strength ratio ζ_1/ζ_2 for the radius ratios $R_1/R_2 = 1/2$, $R_1/R_2 = 1/3$, and $R_1/R_2 = 1/4$. We have classified the resulting interactions using the scheme devised by Dritschel and Waugh (1992). The structures are categorized into the "Concentric", "Tripole", "Merger", and "Elastic Interaction" regimes. All calculations were performed on the f-plane. The abscissa in the two-dimensional parameter space in Fig. 10 is the dimensionless gap $\triangle/R_1$, which ranges from 0 to 4, and the ordinate is the vorticity strength ratio γ, which ranges from 1 to 10. Figure 10 suggests that the demarcation zone between the concentric vorticity regime and the merger type regime is around $\gamma = 5$. The tripole vortex structure is a distinct feature in the demarcation zone. Concentric vorticity structures are favored when γ is greater than 5. With $\gamma = 6$, concentric vorticity structures occur when the dimensionless gap $(\triangle/R_1)$ ranges from 0.5 to 3.5. The range of the dimensionless gap $(\triangle/R_1)$ for the concentric vorticity structure extends from 0 to 3.5 for a γ larger than 7. Of particular interest in the diagram is that when γ is larger than 8, formation of a concentric vorticity structure requires a separation distance between the neighboring vorticity field and the core vortex that is within three to four times the core vortex radius.

Our simulations suggest that concentric vorticity structures can be a result of binary vortex interaction. The flow fields associated with the strong core vortex provide the necessary stretching which can shear out the weaker vortex into a thin strip of enhanced vorticity wrapped around the core vortex. The formation of concentric vorticity structures requires a very strong core vortex with a vorticity at least six times stronger than the neighboring vortices, a large neighboring vorticity area that is larger than the core vortex, and a separation distance between the neighboring vorticity field and the core vortex that is within three to four times the core vortex

radius. If the separation distance is too small and the core vortex is of only marginal strength, the resultant evolution most likely leads to monopole formation. Tripole vortex formation may result in the case of marginal strength of the core vortex and a relatively small dimensionless gap. When the vortex strength is greater than 8, a concentric vorticity structure can form even when the dimensionless gap is zero initially.

b. multiple vortex interaction and Lekima experiments

We have demonstrated with the binary vortex interaction that concentric vorticity structures can form from a strong, small vortex and a weak, large vortex nearby. The strong, small vortex serves as the "organizer" of the surrounding vortices (the "satellites") into the concentric vorticity structure. The purpose of studying multiple vortex interactions is to investigate if there is a preferred surrounding vortex size (or preferred background vorticity spatial scale) for the formation of the concentric vorticity structure when the core vortex is of sufficient strength. Specifically, we consider the same total vorticity but in different sizes in the satellites. The top row in Fig. 11 gives the benchmark binary vortex interaction for comparison with the multiple vortex interactions. The benchmark binary vortex interaction has the vorticity strength ratio $\gamma = 10$, the vortex radius ratio $r = 1/4$, and the dimensionless gap $\triangle/R_1 = 1.0$. The binary vortex interaction produces a concentric vorticity structure in the 12-hour simulation. We then use the same core vortex but split the surrounding vortex into two, four, and eight equal size satellite vortices. The total vorticity in these satellites is the same as the vorticity in the benchmark satellite. Figure 11 shows that concentric vorticity structures form in all of the multiple vortex interactions with two, four, and eight satellites. Other experiments

with different patterns of the satellites (not shown) also yielded similar concentric vorticity structures.

Figure 12 is similar to the multiple vortex experiments in Fig. 11 except the core is now surrounded by 9 and 16 equal-size satellite vortices. The first two experiments are for the 9-symmetric-satellite orientations with respect to the core organizer. The simulation in the first row in Fig. 12 suggests that formation of a concentric vorticity structure. The second row in Fig. 12, with 9 symmetric satellites farther away from the core ($\triangle/R_1 = 4.5$), shows insufficient straining out at hour 3 as compared to the first case. The subsequent evolution of the second row does not favor the formation of a concentric vorticity structure. The 9-satellite experiments suggest that even a symmetric initial satellite distribution does not guarantee a concentric vorticity structure if the separation distance is too large (e.g. $\triangle/R_1 = 4.5$). In the case where the symmetric satellites are too far away, there will be a weaker straining out effect on the satellite vortices by the core organizer, as well as insufficient stabilization by the core organizer vortex. The third and fourth rows in Fig. 12 are for a 16-satellite initial condition. Note that the surrounding vortices in the 16-satellite cases have the same radius as the core vortex. The symmetric 16-satellite vortex experiment (the third row) involves an initial condition where the centers of the 16 satellites were on two concentric circles (6 on the inner circle and 9 on the outer circle). The figure shows that a concentric vorticity structure formed on the inner circle while the vortices on the outer circle failed to form a secondary outer band. The asymmetric 16-satellite case (the fourth row) failed to produce a concentric vorticity structure. We have also tested the 16-satellite initial condition in other asymmetric configurations and also with a very small diffusion (not shown) and found no concentric vorticity structures. These results, in agreement with our binary experiments, support the notion that no concentric vorticity structure forms

with satellite vortices of the same radius as the core. The only exception to this is when the initial 16 satellites are symmetric and in a circle close to the core vortex.

A summary of the multiple vortex experiments indicates that there is a preferred threshold scale of the surrounding vorticity for the formation of the concentric vorticity structure. The surrounding vorticity patches should be larger than the core vortex. Figure 13 shows the tangential wind speed for radial arms toward the west and south that emanate from the vortex center at different times for the experiment in the second row of Fig. 11. The wind profiles show clearly a secondary maxima in the tangential wind field contracting with time in these different radial arms. Figure 13 also suggests the asymmetric nature of the contraction, as the initial satellite vortices are located only on the west and south arms of the organizer vortex. The time and spatial scales of the secondary wind maximum contraction in Fig. 13 are in general agreement with the observations in Hurricane Gilbert (BW92). The contraction mechanism for the outer bands is often argued to be a balanced response to an axisymmetric ring of convective heating (Shapiro and Willoughby 1982 and Schubert and Hack 1982). Our results in Fig. 13 suggest that the nonlinear advective dynamics involved in the straining out of a large, weak vortex into a concentric vorticity band can also result in the contraction of the secondary wind maximum .

Our final experiments involve a core organizer vortex and the surrounding vorticity field that resembles the shape of the convection observed in the Lekima radar picture. Figure 14 shows sensitivity experiments for the vorticity field at hour 0, 3, 6 and 12 for these experiments. The control experiment on the top row in Fig. 14 has the vorticity strength ratio $\gamma = 7.5$ and the shortest distance from the outer vorticity boundary to the core vortex boundary is $\triangle/R_1 = 0.6$ ($R_1 = 10$ km). The value $\gamma = 7.5$ is estimated from the radar radial wind and core vortex and with the assumption that the typical vorticity induced by convection is about ten times

the local Coriolis parameter. The control experiment produces a concentric vorticity structure within 12 hours. The second row in Fig. 14 is a similar experiment but with the parameter $\triangle/R_1 = 0$. In this experiment we find that a monopole results, possibly due to insufficient negative vorticity being advected inward to provide a shield from the inward mixing of the outer vorticity field. The third row of Fig. 14 is the same as the top row except that $\gamma = 3$. A monopole vortex is formed instead of a concentric vorticity structure in this experiment. The result is in agreement with the binary vortex interaction in the sense that the core strength is most vital not only to serve as an organizer but also to resist the merger process into a monopole. The last row of Fig. 14 shows the results of an experiment with $\triangle/R_1 = 2.8$ and $\gamma = 3$. In this case the core vortex at the center of a circle is approximately surrounded by the inner boundary of the outer vorticity field. Consistent with the binary vortex interaction, the weak core vortex cannot maintain a concentric vorticity structure and it eventually becomes a monopole vortex.

4. Concluding Remarks

There are many documented cases of binary tropical cyclone interactions that resemble the theoretical work of Dritschel and Waugh (1992) (e.g., see Larson 1975, Lander and Holland 1993, Kuo et al. 2000, Prieto et al. 2003). The complete straining out regime of the binary vortex interaction in Dritschel and Waugh (1992) shows a small, weaker vortex being sheared out into thin filaments of vorticity surrounding the large, stronger vortex with no incorporation into the large vortex. The regime resembles the concentric vorticity structure except the filaments are too thin to be called a concentric eyewall. Furthermore, Typhoon Lekima observations indicate that it is a huge area of convection with weak cyclonic vorticity outside the core vortex that wraps around the inner eyewall, rather than the other way around. This large vortex forms the outer band on a time scale of 12 hours. The interaction of a small and strong vortex with a large and weak vortex was not studied by Dritschel and Waugh (1992) as their vortices are of the same strength and their larger vortex was always the "victor" and the smaller vortex was the one often being partially or totally destroyed. An extension of the complete straining out regime to include a finite-width outer band is needed to explain the interaction of a small and strong vortex (representing the tropical cyclone core) with a large and weaker vortex (representing the vorticity induced by the moist convection outside the central vortex of a tropical cyclone). With the introduction of a parameter of vorticity strength ratio into the binary vortex interaction problem, we have added a new dimension to the Dritschel-Waugh vortex interaction scheme that provides a proper concentric vorticity structure as well as the tripole vortex structure.

The vorticity strength of the central core vortex is essential in the formation of a concentric vorticity structure. It has to be at least six times stronger than the neighboring vortices. In addition, the neighboring vorticity area must be larger

than the core vortex and with a separation distance from the core vortex that is within three to four times the core vortex radius. The contraction of the secondary tangential wind maximum and the formation of the moat are salient features of the binary vortex interaction. The contraction of the secondary tangential wind maximum is in general agreement with the aircraft observations that show the contraction of the outer tangential wind maximum from a distance of 100 km to 50 km on a time scale of approximately twelve hours (BW92). No diabatic heating is required in the present contraction mechanism. Diabatic heating, however, may be crucial in the enhancement of the secondary tangential wind maximum during the symmetrization of the asymmetric convection. The negative vorticity anomaly in the moat serves as a barrier to the further inward mixing of the outer vorticity field. The moat in our model is caused by the strong differential rotation associated with the core vortex and the advective organization of the negative vorticity anomalies. In nature, the strong subsidence induced by the intensified eyewall convection may also contribute to the formation of the moat (Dodge et al. 1999). Rozoff et al. (2003) hypothesized that both subsidence and rapid filamentaion are important to the dynamics of the moat. All these arguments agree with the fact that the concentric eyewalls often form when the tropical cyclone is of sufficient strength.

The concentric vorticity structures in our barotropic numerical experiments are quite robust and can maintain themselves for more than 24 hours after formation. No inner vortex replacement cycle is modeled in our initial value problems. Presumably, a high-resolution "full-physics model" to take into account the moisture cutoff process is required to simulate the eyewall replacement process. With simple model calculations, our intent is not to deprecate the importance of the moist physics, but rather to isolate the fundamental dynamics that may be responsible for the concentric vorticity structure formation. Our arguments may be applicable

to the formation of concentric eyewalls if the time scale of the core vortex intensity modification is longer than the time scale of the concentric vorticity formation. Without detailed observations of the potential vorticity distribution in the eyewall evolution to compare with, our results may remain suggestive. However, it does not seem unreasonable to expect the pivotal role of the strength of the inner core vortex in maintaining itself, in stretching, organizing and stabilizing the outer vorticity field, and the shielding effect of the moat to prevent further merger and enstrophy cascade processes in concentric eyewall dynamics.

Acknowledgments This research was supported by the National Research Council of Taiwan NSC91-2111-M-002-020 and NSC92-2625-Z-002-002 to National Taiwan University, and National Science Foundation, under Grant ATM 0101135 to the Naval Postgraduate School. We would like to thank Wayne Schubert, Hugh Willoughby, and an anonymous reviewer for their useful comments and suggestions.

REFERENCES

Batchelor, G. K., 1969: Computation of the energy spectrum in homogeneous two-dimensional turbulence. *Phys. Fluids Suppl. II*, **12**, 233–239.

Black, M. L., and H. E. Willoughby, 1992: The concentric eyewall cycle of Hurricane Gilbert. *Mon. Wea. Rev.*, **120**, 947–957.

Bowman, K. P., 1996: Rossby wave phase speeds and mixing barriers in the stratosphere. Part I: Observations. *J. Atmos. Sci.*, **53**, 905–916.

Cushman-Roisin, B., 1994: *Introduction to Geophysical Fluid Dynamics.* Prentice Hall, Englewood Cliffs, New Jersey, 320pp.

DeMaria, M., and C. L. Chan, 1984: Comments on "A numerical study of the interactions between two tropical cyclones." *Mon. Wea. Rev.*, **112**, 1643–1645.

Dodge, P., R. W. Burpee, and F. D. Marks Jr., 1999: The kinematic structure of a hurricane with sea level pressure less than 900 mb. *Mon. Wea. Rev.*, **127**, 987–1004.

Dritschel, D. G., 1989: On the stabilization of a two-dimensional vortex strip by adverse shear. *J. Fluid Mech.*, **206**, 193–221.

Dritschel, D. G., 1995: A general theory for two-dimensional vortex interactions. *J. Fluid Mech.*, **293**, 269–303.

Dritschel, D. G., and D. W. Waugh, 1992: Quantification of the inelastic interaction of unequal vortices in two-dimensional vortex dynamics. *Phys. Fluids*, **A4**, 1737–1744.

Hoose, H. M., and J. A. Colón, 1970: Some aspects of the radar structure of Hurricane Beulah on September 9, 1967. *Mon. Wea. Rev.*, **98**, 529–533.

Kossin, J. P., W. H. Schubert, and M. T. Montgomery, 2000: Unstable interaction between a hurricane's primary eyewall and a secondary ring of enhanced vorticity. *J. Atmos. Sci.*, **57**, 3893–3917.

Kuo, H.-C., G. T.-J. Chen, and C.-H. Lin, 2000: Merger of tropical cyclones Zeb and Alex. *Mon. Wea. Rev.*, **128**, 2967–2975.

Kuo, H.-C., R. T. Williams, and J.-H. Chen, 1999: A possible mechanism for the eye rotation of Typhoon Herb. *J. Atmos. Sci.*, **56**, 1659-1673.

Lander, M. and G. J. Holland, 1993: On the interaction of tropical-cyclone-scale vortices. I: Observations. *Quart. J. Roy. Meteor. Soc.*, **119**, 1347–1361.

Larson, R. N., 1975: Picture of the month – Hurricane twins over the Eastern North Pacific Ocean. *Mon. Wea. Rev.*, **103**, 262–265

McIntyre, M. E., 1989: On the Antarctic ozone hole. *J. Atmos. Terr. Phys.*, **51**, 29–43.

McWilliams, J. C., 1984: The emergence of isolated coherent vortices in turbulent flow. *J. Fluid Mech.*, **146**, 21–43.

Montgomery, M. T., and R. J. Kallenbach, 1997: A theory for vortex Rossby-waves and its application to spiral bands and intensity changes in hurricane. *Quart. J. Roy. Meteor. Soc.*, **123**, 435–465.

Nong, S., and K. A. Emanuel, 2003: A numerical study of the genesis of concentric eyewalls in hurricane. *Quart. J. Roy. Meteor. Soc.*, **129**, in press.

Polvani L. M., and R. A. Plumb, 1992: Rossby wave breaking, microbreaking, filamentation, and secondary vortex formation: the dynamics of a perturbed vortex. *J. Atmos. Sci.*, **49**, 462–476.

Prieto, R., J. P. Kossin, and W. H. Schubert, 2001: Symmetrization of lopsided vorticity monopoles and offset hurricane eyes. *Quart. J. Roy. Meteor. Soc.*, **127**, 1–17.

Prieto, R., B. D. McNoldy, S. R. Fulton, and W. H. Schubert, 2003: A classification of binary tropical-cyclone-like vortex interactions. *Mon. Wea. Rev.*, **131**, 2656–2666.

Reasor, P. D., M. T. Montgomery, F. D. Marks, and J. F. Gamache, 2000: Low-wavenumber structure and evolution of the hurricane inner core observed by airborne dual-Doppler radar. *Mon. Wea. Rev.*, **128**, 1653-1680.

Ritchie, E. A., and G. J. Holland, 1993: On the interaction of tropical-cyclone scale vortices. II: Interacting vortex patches. *Quart. J. Roy. Meteor. Soc.*, **119**, 1363–1379.

Rozoff, C. M., W. H. Schubert, B. D. McNoldy, and J. P. Kossin, 2003: Rapid filamentation zones in intense tropical cyclones. *J. Atmos. Sci.*, **60**, submitted.

Schubert, W. H., and J. J. Hack, 1982: Inertial stability and tropical cyclone development. *J. Atmos. Sci.*, **39**, 1687–1697.

Schubert, W. H., M. T. Montgomery, R. K. Taft, T. A. Guinn, S. R. Fulton, J. P. Kossin, and J. P. Edwards, 1999: Polygonal eyewalls, asymmetric eye contraction, and potential vorticity mixing in hurricanes. *J. Atmos. Sci.*, **56**, 1197–1223.

Shapiro, L. J., and H. E. Willoughby, 1982: The response of balanced hurricanes to local sources of heat and momentum. *J. Atmos. Sci.*, **39**, 378–394.

Willoughby, H. E., J. M. Masters, and C. W. Landsea, 1989: A record minimum sea level pressure observed in Hurricane Gilbert. *Mon. Wea. Rev.*, **117**, 2824–2828.

Willoughby, H. E., 1990: Temporal changes of the primary circulation in tropical cyclones. *J. Atmos. Sci.*, **47**, 242–264.

Willoughby, H. E., J. A. Clos, and M. Shoreibah, 1982: Concentric eye walls, secondary wind maxima, and the evolution of the hurricane vortex. *J. Atmos. Sci.*, **39**, 395-411.

Figure Captions

Figure 1a. Reflectivity at 0.5 elevation angle for Typhoon Lekima (2001) from the Central Weather Bureau WSR-88D (10 cm) radar at Kung-Ting for the period 0935 September 25 to 1935 September 25. The sequence of the images is from left to right and from top to bottom. The time interval between each image is approximately 75 min. The local time of observation is indicated on top of each image. The radial increment of the circles centered at radar station is 50 km. The nine images illustrate the formation of a concentric eyewalls.

Figure 1b. Similar to Fig. 1a except for the radial wind observations.

Figure 2. Initial configuration of two circular vortices with radii R_1 and R_2 ($R_1 < R_2$), vorticity ζ_1 and ζ_2 ($\zeta_1 > \zeta_2$), and the gap $\triangle$.

Figure 3. The sensitivity of the vorticity field in the binary vortex experiments with respect to the vorticity strength ratio (γ) at hour 0, 3, 6, and 12 with the dimensionless gap $\triangle/R_1 = 1$, and the vortex radius ratio $r = 1/3$.

Figure 4. The sensitivity of the vorticity field in the binary vortex experiments with respect to the dimensionless gap $\triangle/R_1$ at hour 0, 3, 6, and 12 with the vorticity strength ratio ($\gamma = 5$) and the vortex radius ratio $r = 1/3$.

Figure 5. The sensitivity of the vorticity field in the binary vortex experiments with respect to the vortex radius ratio r at hour 0, 3, 6, and 12 with the vorticity strength ratio ($\gamma = 5$) and the dimensionless gap $\triangle/R_1 = 1$.

Figure 6. Similar to Fig. 5 except that the dimensionless gap $\triangle/R_1 = 0$ and the vorticity strength ratio $\gamma = 10$.

Figure 7. The sensitivity of the vorticity field in the binary vortex experiments with respect to the diffusivity ν at hour 0, 6, 12, and 36 with the vorticity strength ratio ($\gamma = 5$),vortex radius ratio $r = 1/3$ and the dimensionless gap $\triangle/R_1 = 2.5$.

Figure 8. Time dependence of (a) kinetic energy and enstrophy, and (b) palinstrophy for experiments in Fig. 8.

Figure 9. The sensitivity of the vorticity field in the binary vortex experiments with the core vortices possess the same maximum wind but different radius and vorticity field. Two vortices considered have the vorticity and radius of (1.5×10^{-2} s^{-1}, 10 km) and (0.75×10^{-2} s^{-1}, 20 km) respectively. The dimensionless gap is 1 in the experiments. The outer vortices considered have the radius of 30 km and 40 km respectively.

Figure 10. Summary of numerical experiments with the parameters of the vorticity strength ratio (γ), the dimensionless gap $\triangle/R_1$, and the vortex radius ratio r. The structures are categorized into the C (concentric), T (tripole), M (complete or partial merger), and EI (elastic interaction) regimes .

Figure 11. The top row is the benchmark for the multiple vortex experiments from the binary vortex experiment with the vorticity strength ratio ($\gamma = 10$), vortex radius ratio $r = 1/4$ and the dimensionless gap $\triangle/R_1 = 1.0$. The bottom rows are the multiple vortex interactions with the same core vortex as the benchmark binary vortex interaction. The total vorticity in the neighboring vortices is the same as the neighboring vortex in the binary vortex experiment.

Figure 12. The multiple vortex experiments with nine and sixteen neighboring vortices. The total neighboring vorticity is the same as in the benchmark binary vortex experiment.

Figure 13. The tangential wind speed for radial arms toward the west (left portion) and the south (right portion) that emanate from the vortex center at various times for the experiment in the second row of Fig. 11.

Figure 14. The Lekima experiments with a core vortex and an area of weak vorticity that resembles of the shape of convection as observed in the radar picture. The control experiment on the top row has the vorticity strength ratio $\gamma = 7.5$ and the shortest distance from the outer vorticity boundary to the core vortex boundary is $\triangle/R_1 = 0.6$ ($R_1 = 10$ km). The parameter in second row is the same with the control except with the parameter $\triangle/R_1 = 0$. The parameters in the third row is the same as the control except with $\gamma = 3$. The parameters in the bottom row are $\triangle/R_1 = 2.8$ and $\gamma = 3$.

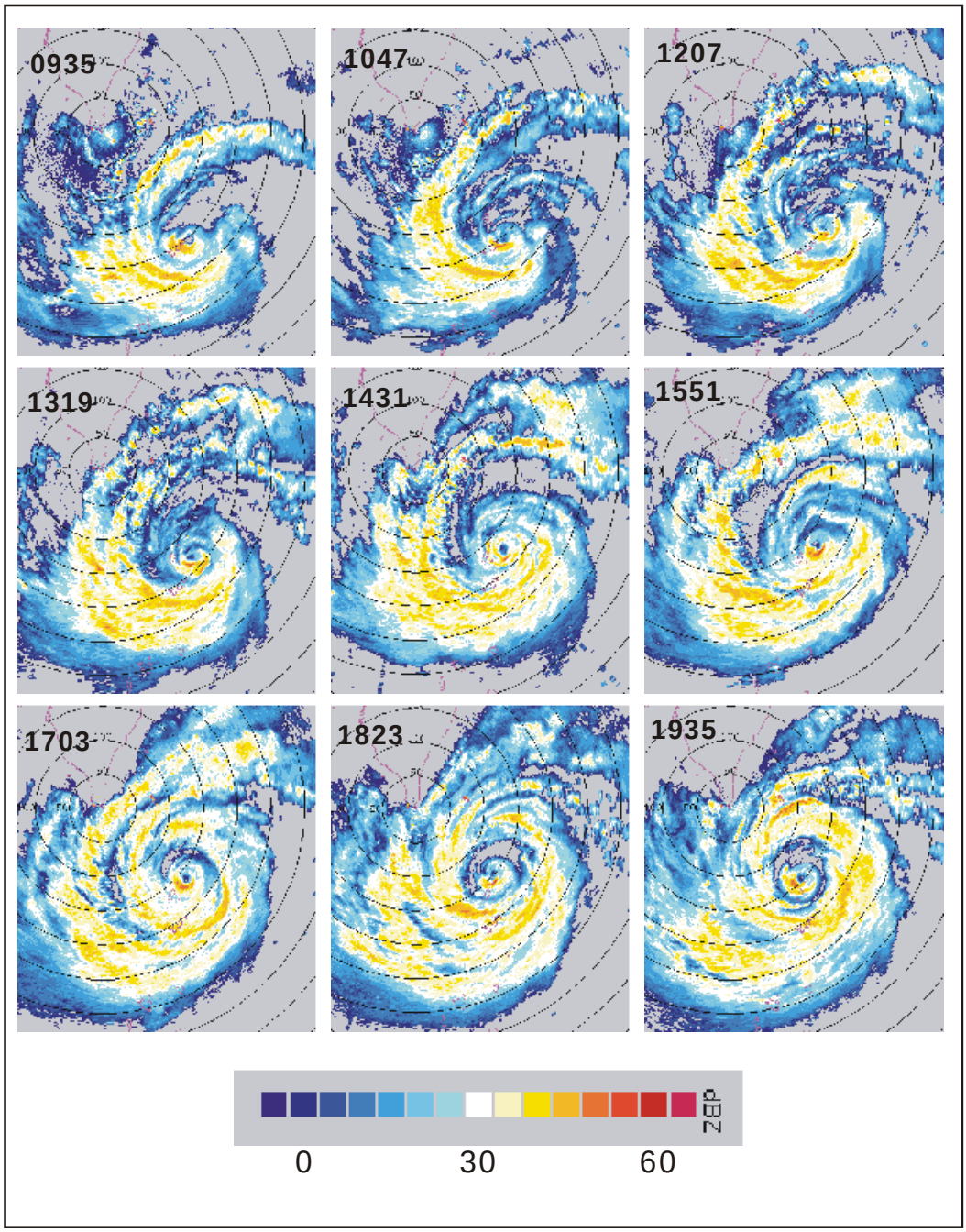

Figure 1a: Reflectivity at 0.5 elevation angle for Typhoon Lekima (2001) from the Central Weather Bureau WSR-88D (10 cm) radar at Kung-Ting for the period 0935 to 1935 September 25. The sequence of the images is from left to right and from top to bottom. The time interval between each image is approximately 75 min. The local time of observation is indicated on top of each image. The radial increment of the circles centered at radar station is 50 km. The nine images illustrate the formation of a concentric eyewalls.

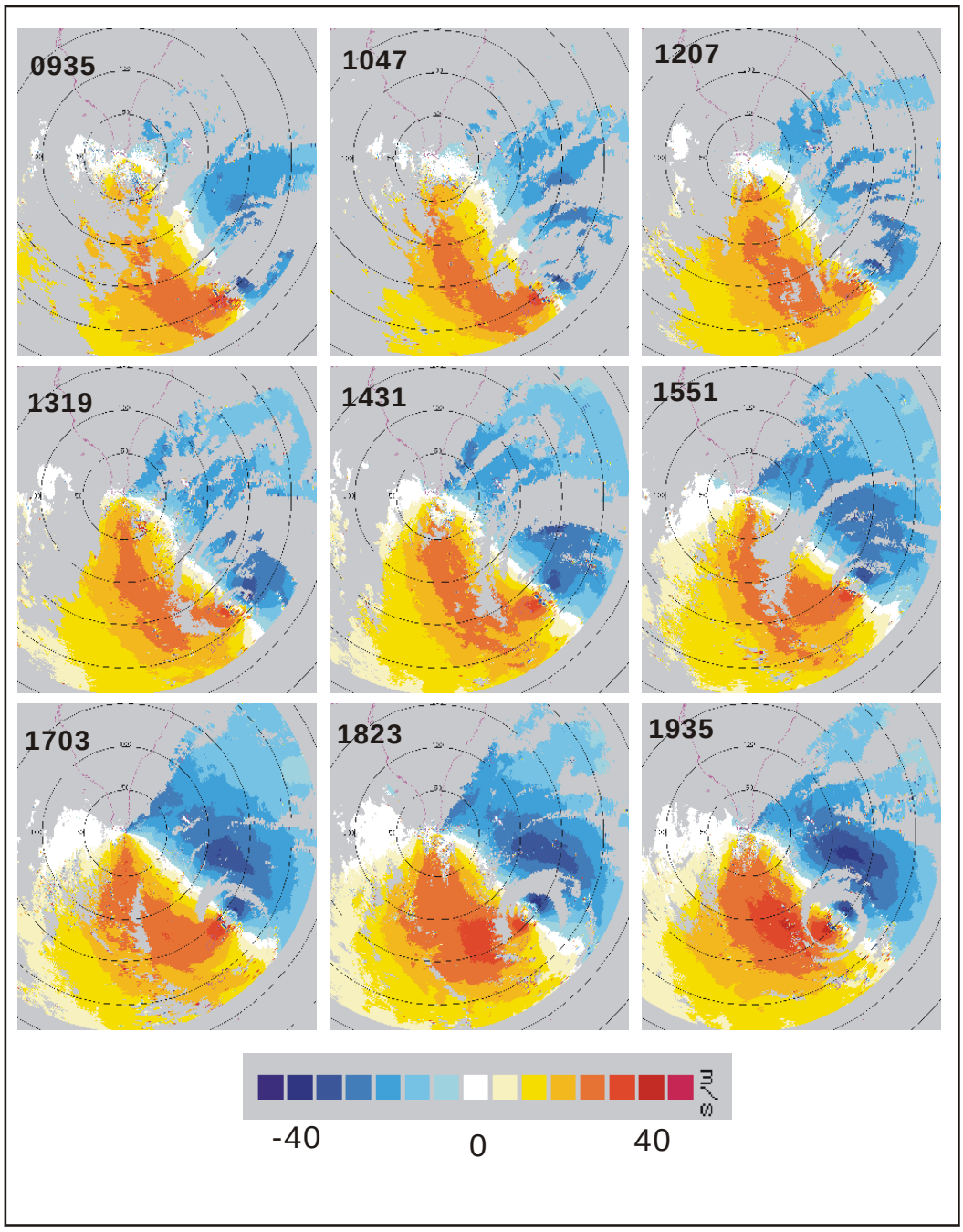

Figure 1b: Similar to Figure 1a except for the radial wind observations.

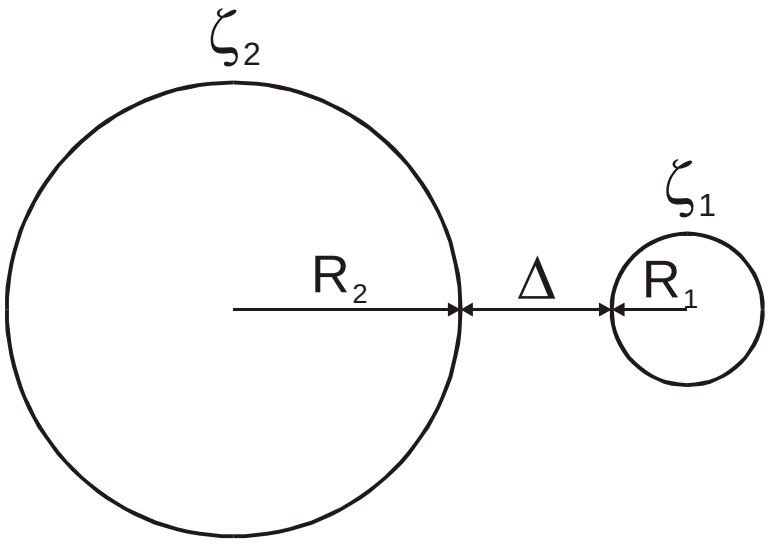

Figure 2: Initial configuration of two circular vortices with radii R_1 and R_2 ($R_1<R_2$), vorticity ζ_1 and ζ_2 ($\zeta_1 > \zeta_2$), and the gap Δ.

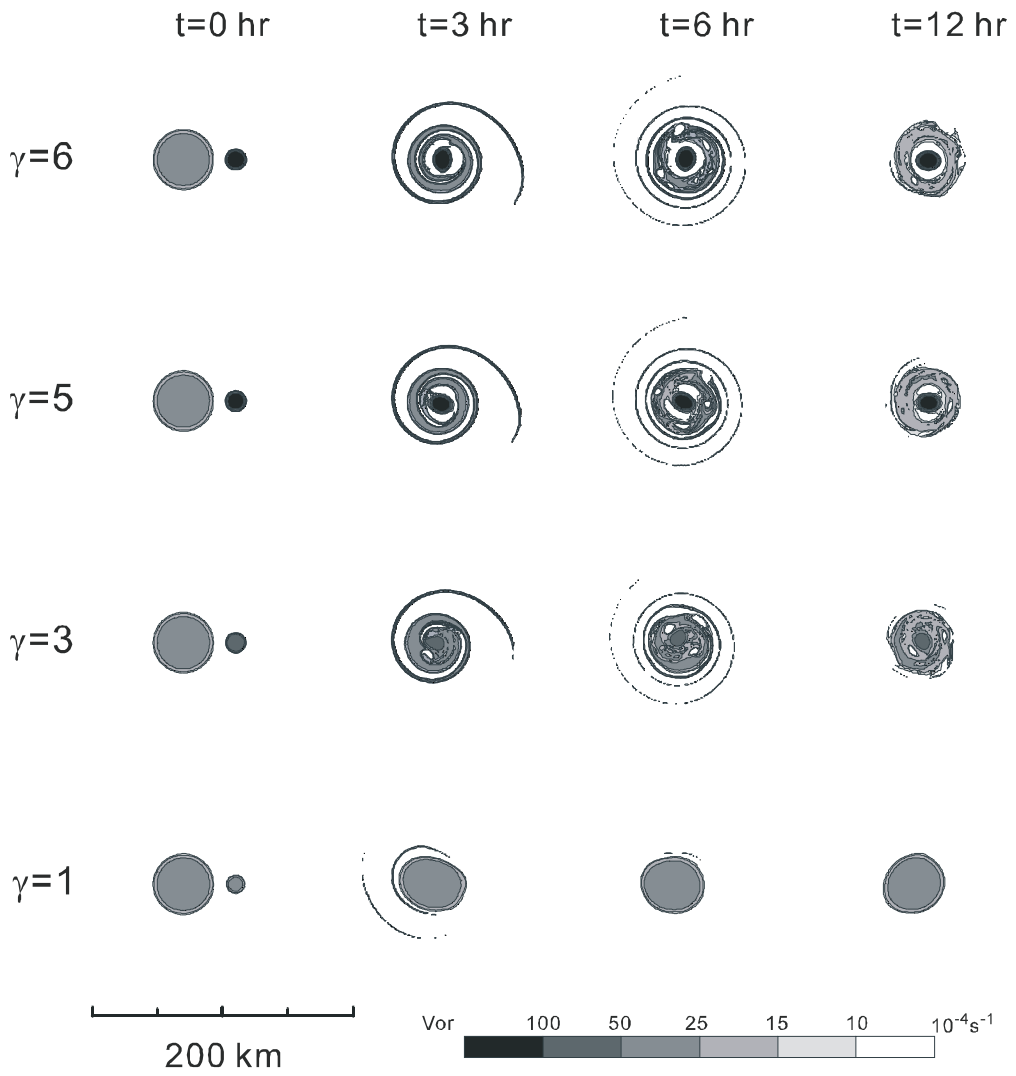

Figure 3: The sensitivity of the vorticity field in the binary vortex experiments with respect to the vorticity strength ratio (γ) at hour 0, 3, 6 and 12 with the dimensionless gap $\Delta/R_1=1$, and the vortex radius ratio r=1/3.

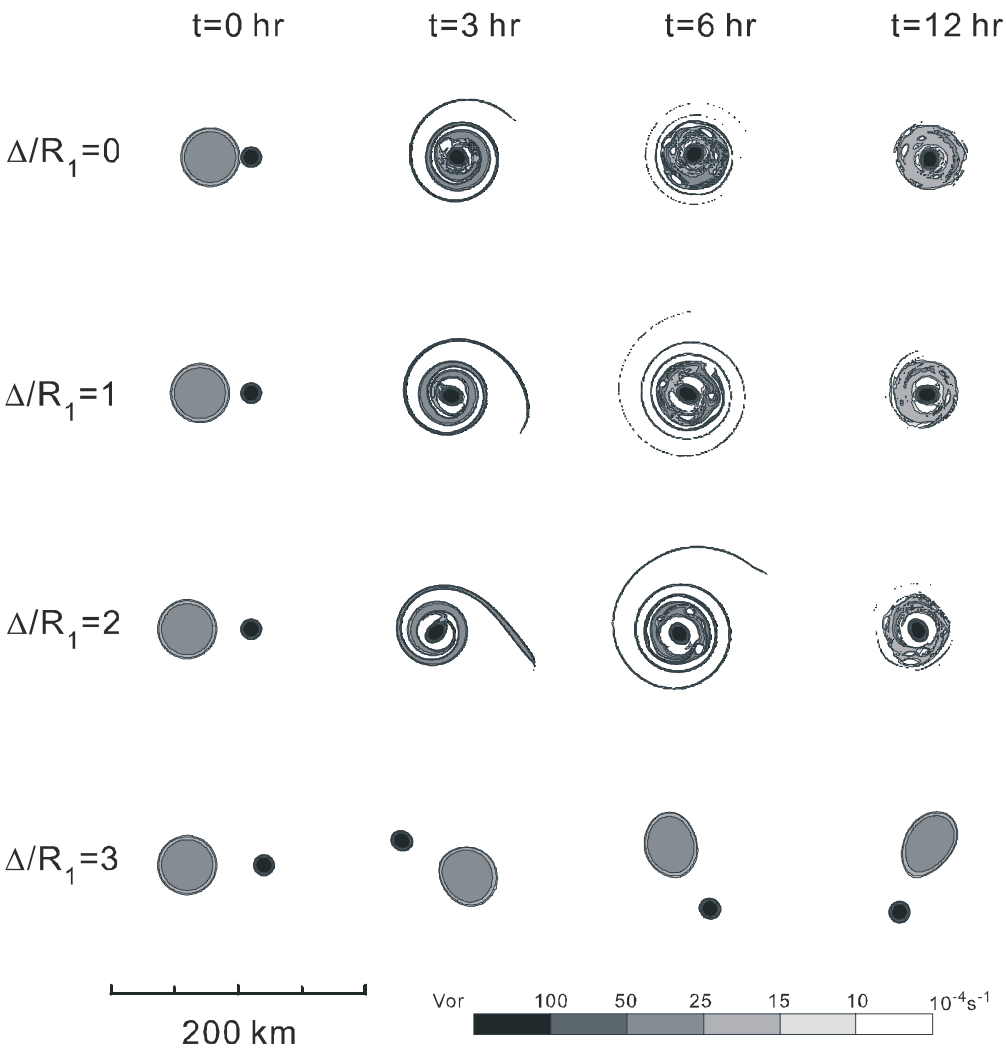

Figure 4: The sensitivity of the vorticity field in the binary vortex experiments with respect to the dimensionless gap (Δ/R_1) at hour 0, 3, 6 and 12 with the vorticity strength ratio γ=5, and the vortex radius ratio r=1/3.

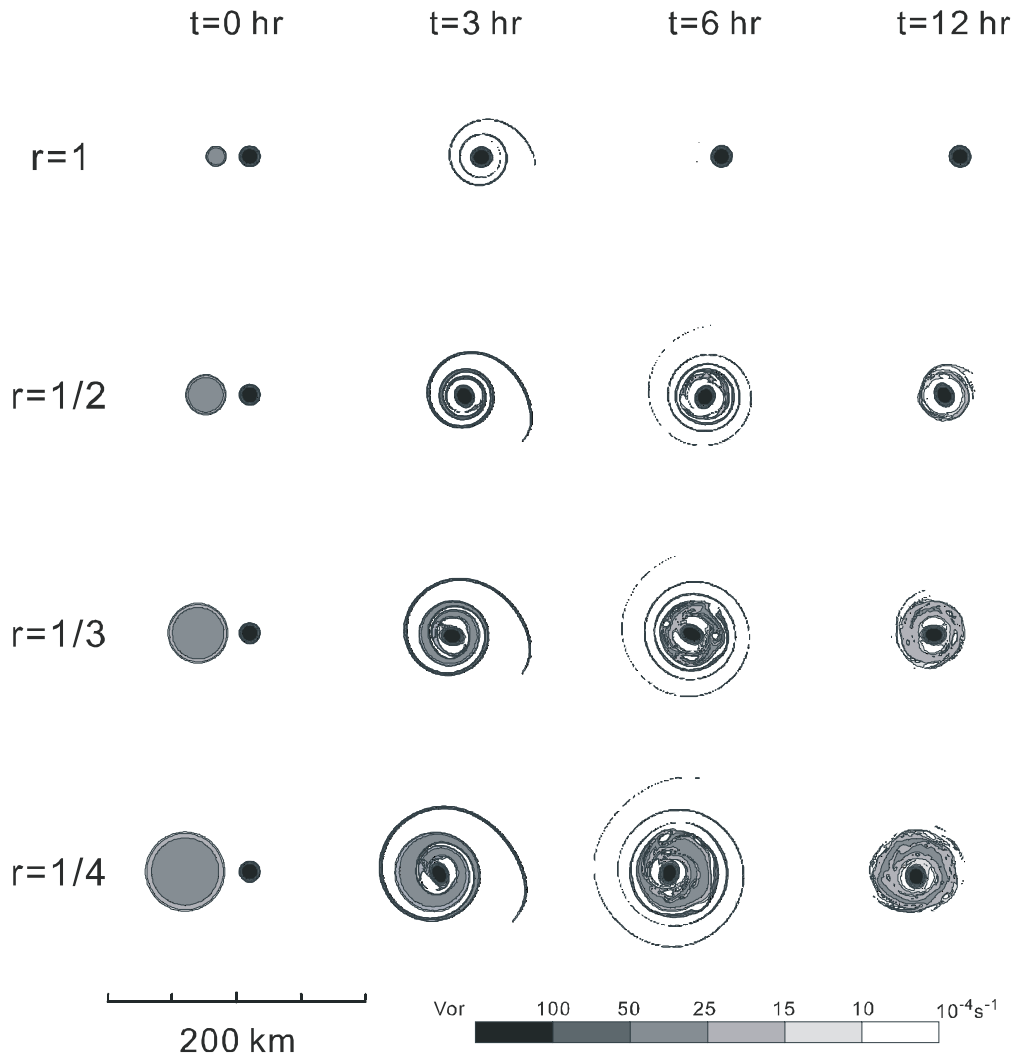

Figure 5: The sensitivity of the vorticity field in the binary vortex experiments with respect to the vortex radius ratio r at hour 0, 3, 6 and 12 with the vorticity strength ratio γ=5, and the dimensionless gap Δ/R_1=1.

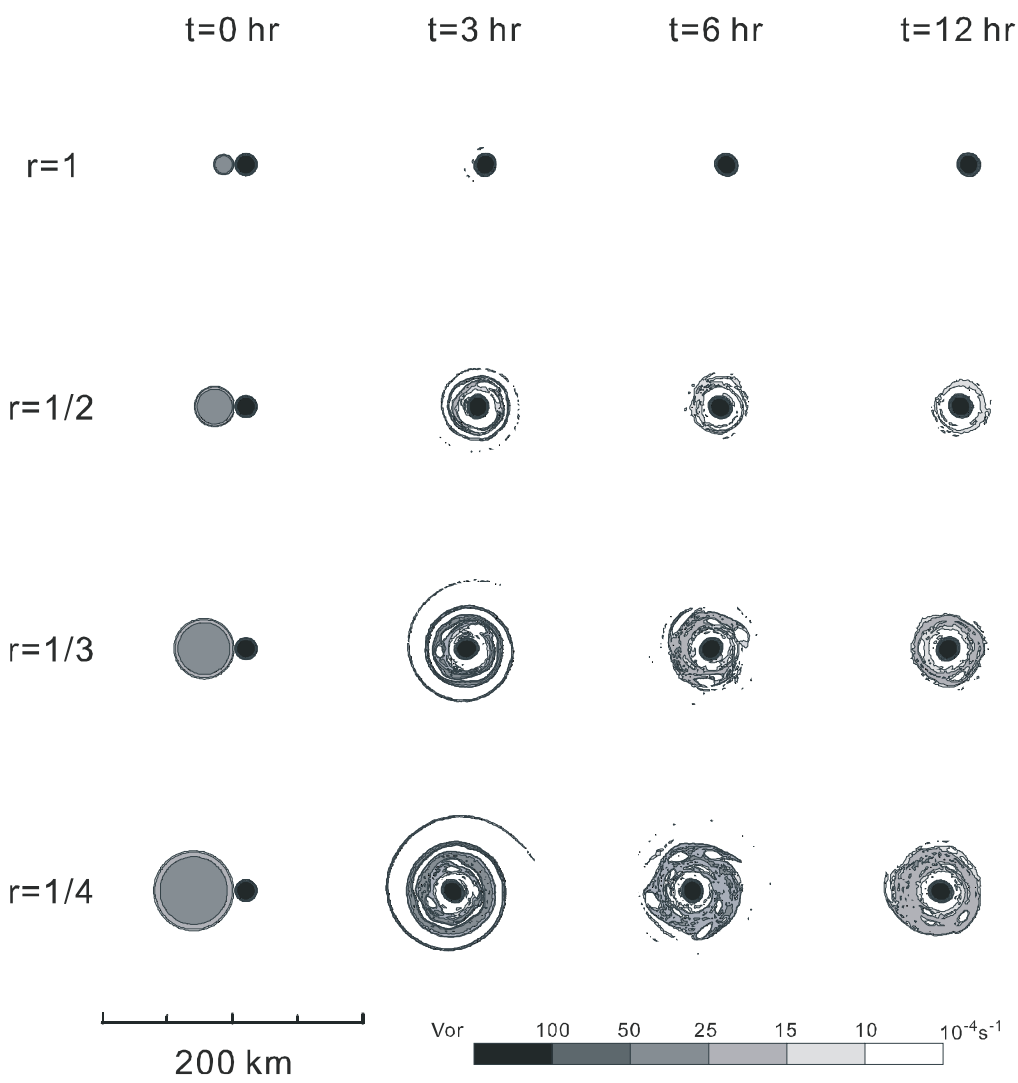

Figure 6: Similar to Figure 5 except that the dimensionless gap $\Delta/R_1=0$ and the vorticity strength ratio $\gamma=10$.

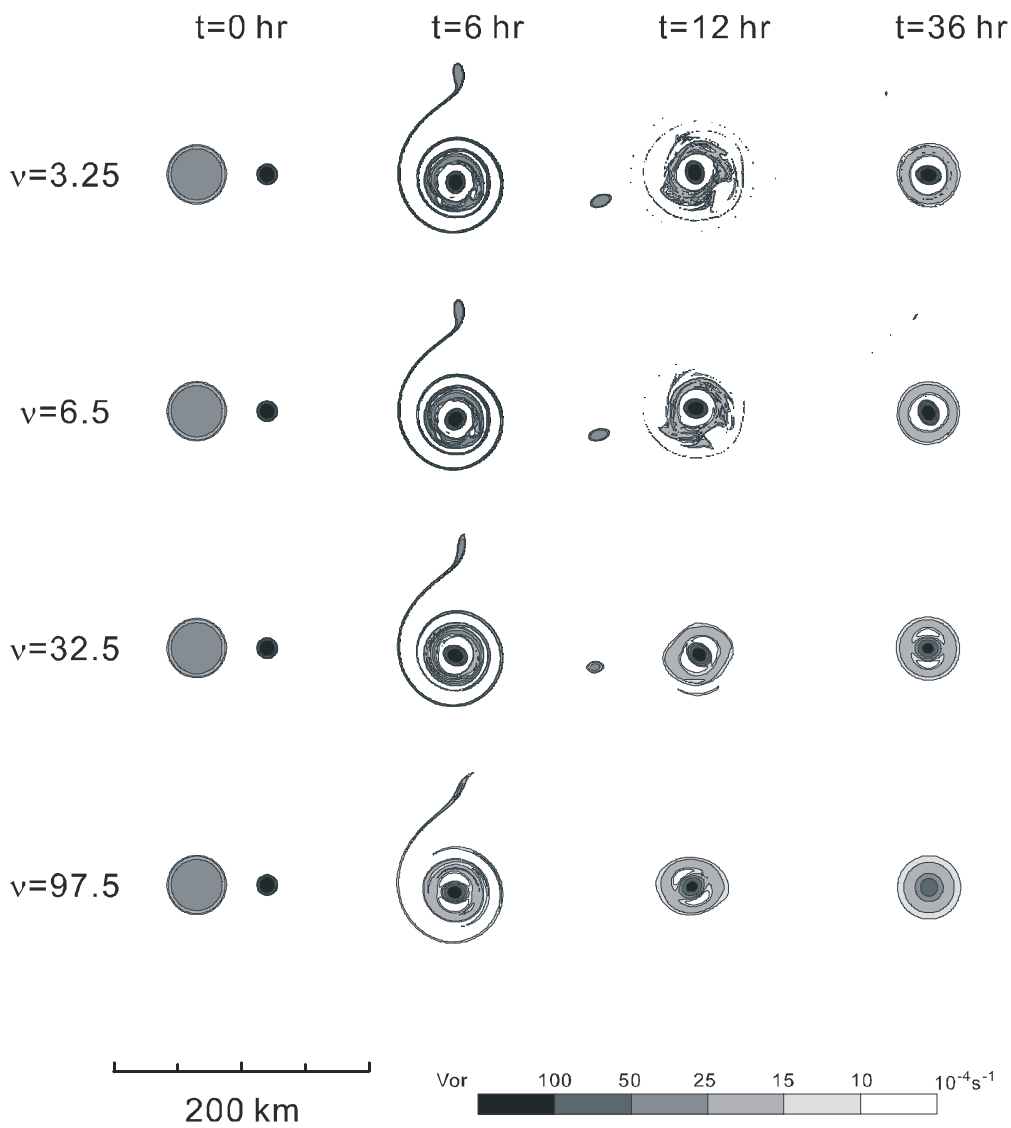

Figure 7: The sensitivity of the vorticity field in the binary vortex experiments with respect to the diffusivity (ν) at hour 0, 3, 6 and 12 with the vorticity strength ratio γ=5, vortex radius ratio r=1/3 and the dimensionless gap Δ/R_1=2.5.

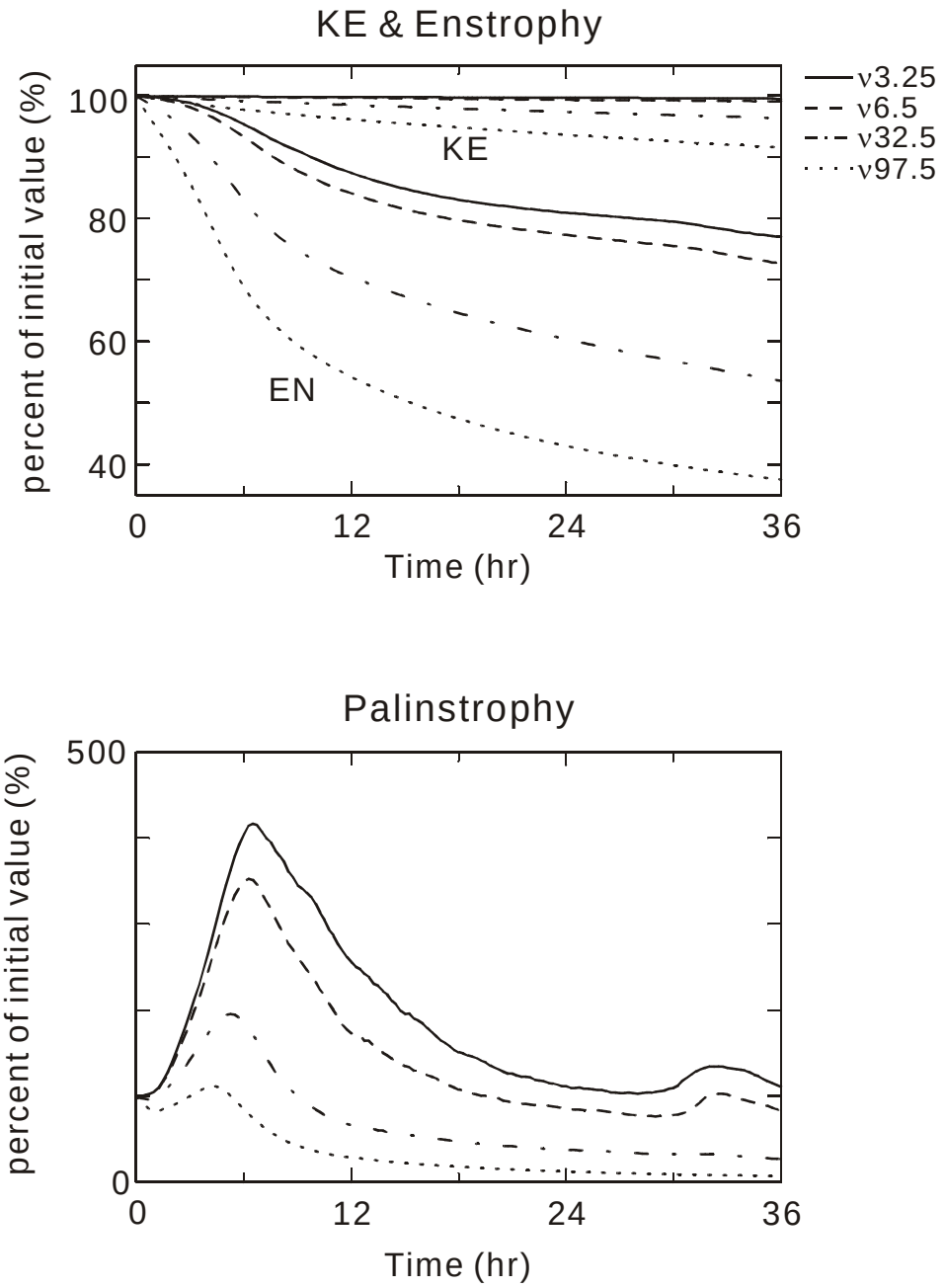

Figure 8: Time dependence of (a) kinetic energy and enstrophy, and (b) palinstrophy for experiments in Figure 7.

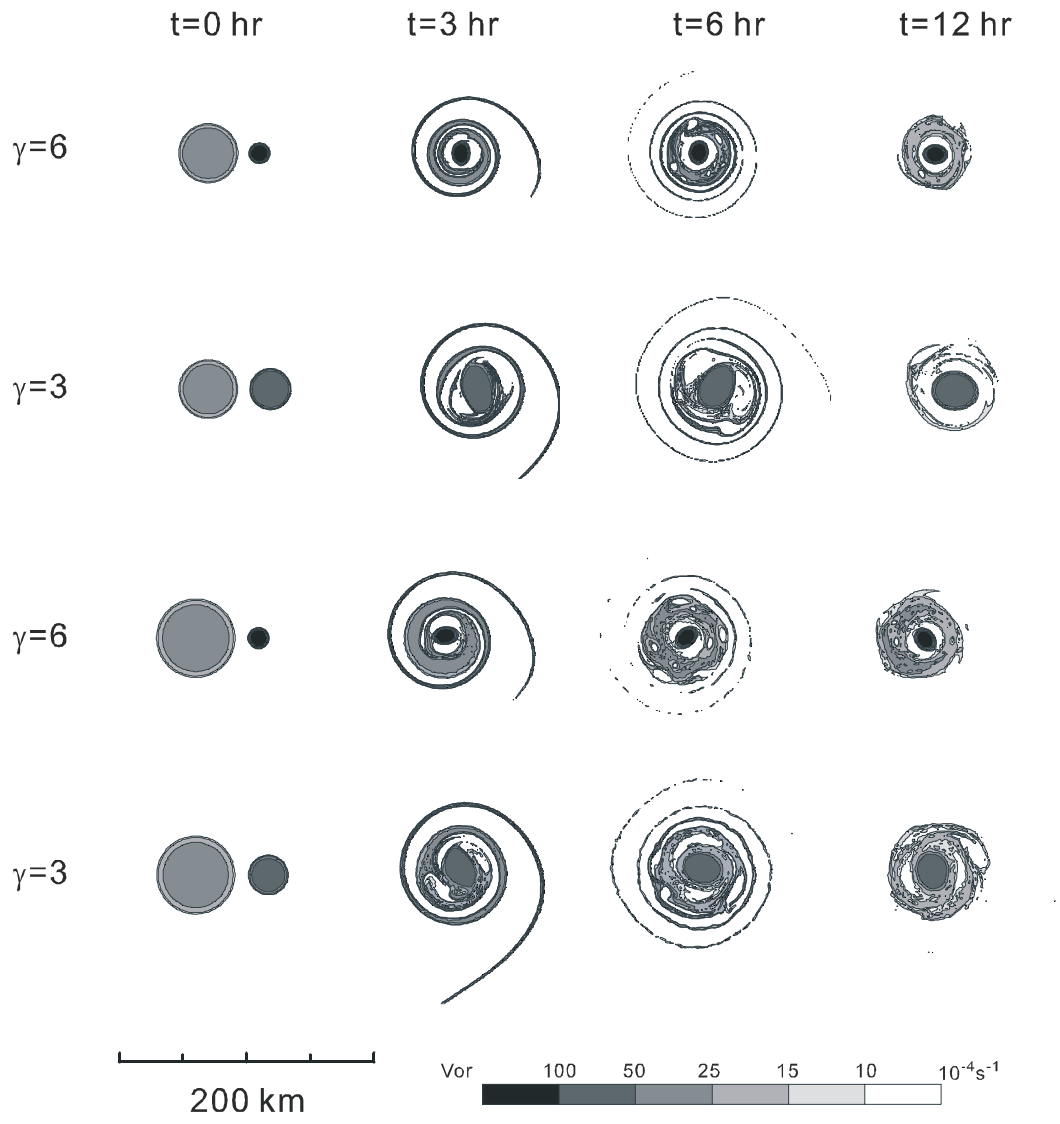

Figure 9: The sensitivity of the vorticity field in the binary vortex experiments with the core vortices process the same maximum wind but different radius of vorticity field. Two core vortices considered have the vorticity and radius of (1.8 × $10^{-2}s^{-1}$, 10 km) and (0.9 × $10^{-2}s^{-1}$, 20 km) respectively. The dimensionless gap is 1 in the experiments. The outer vortices considered have the radius of 30 km and 40 km respectively.

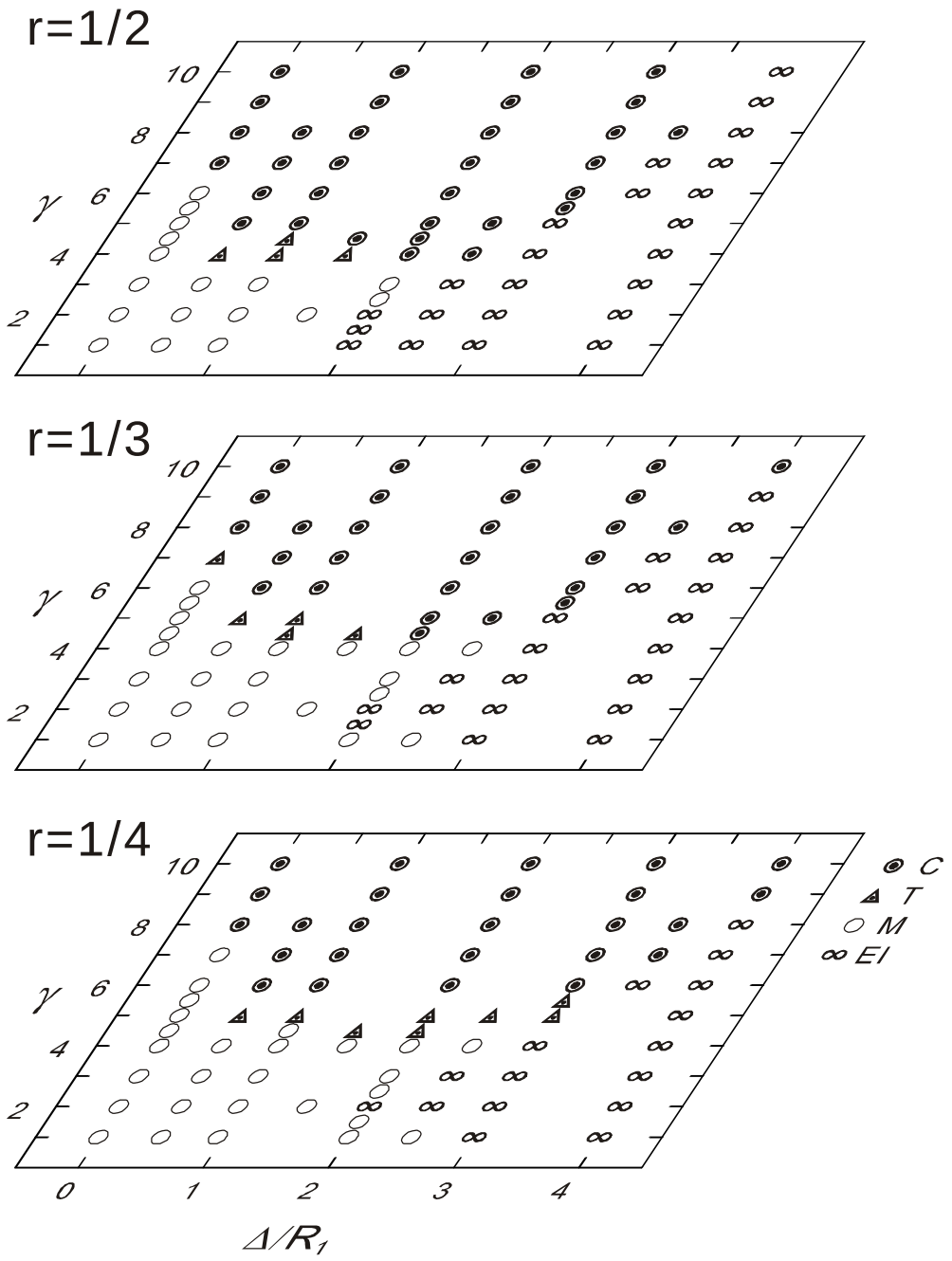

Figure 10: Summary of numerical experiments with the parameters of the vorticity strength ratio (γ), the dimensionless gap Δ/R_1, and the vortex radius ratio r. The structures are categorized into the C (concentric), T (tripole), M (complete or partial merger), and EI (elastic interaction) regimes.

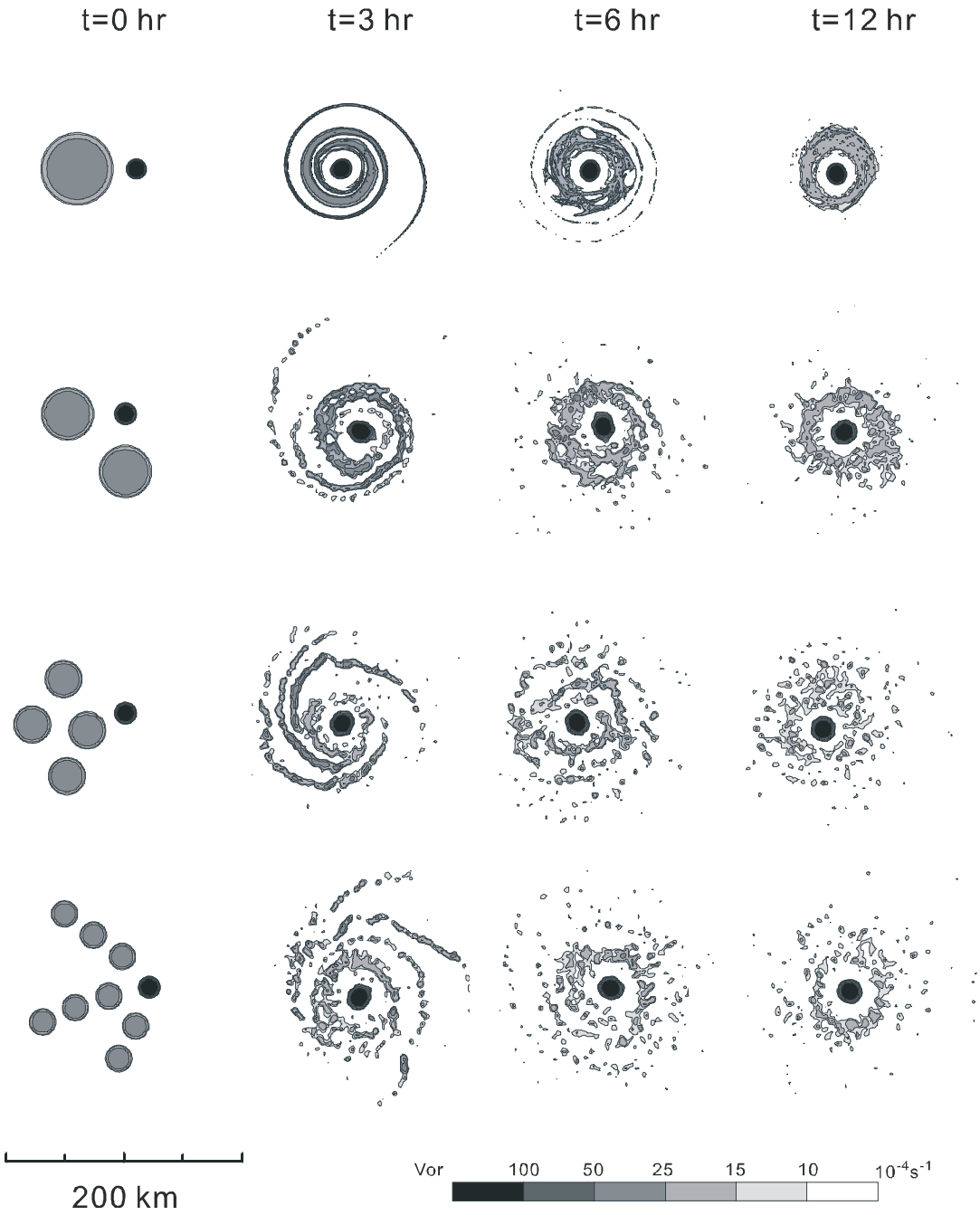

Figure 11: The top row is the benchmark for the multiple vortex experiments from the binary vortex experiment with the vorticity strength ratio γ=10, vortex radius ratio r=1/4, and the dimensionless gap Δ/R_1=1. The bottom rows are the multiple vortex interactions with the same core vortex as the benchmark binary vortex interaction. The total voricity in the neighboring vortices is the same as the neighboring vortex in the binary vortex experiment.

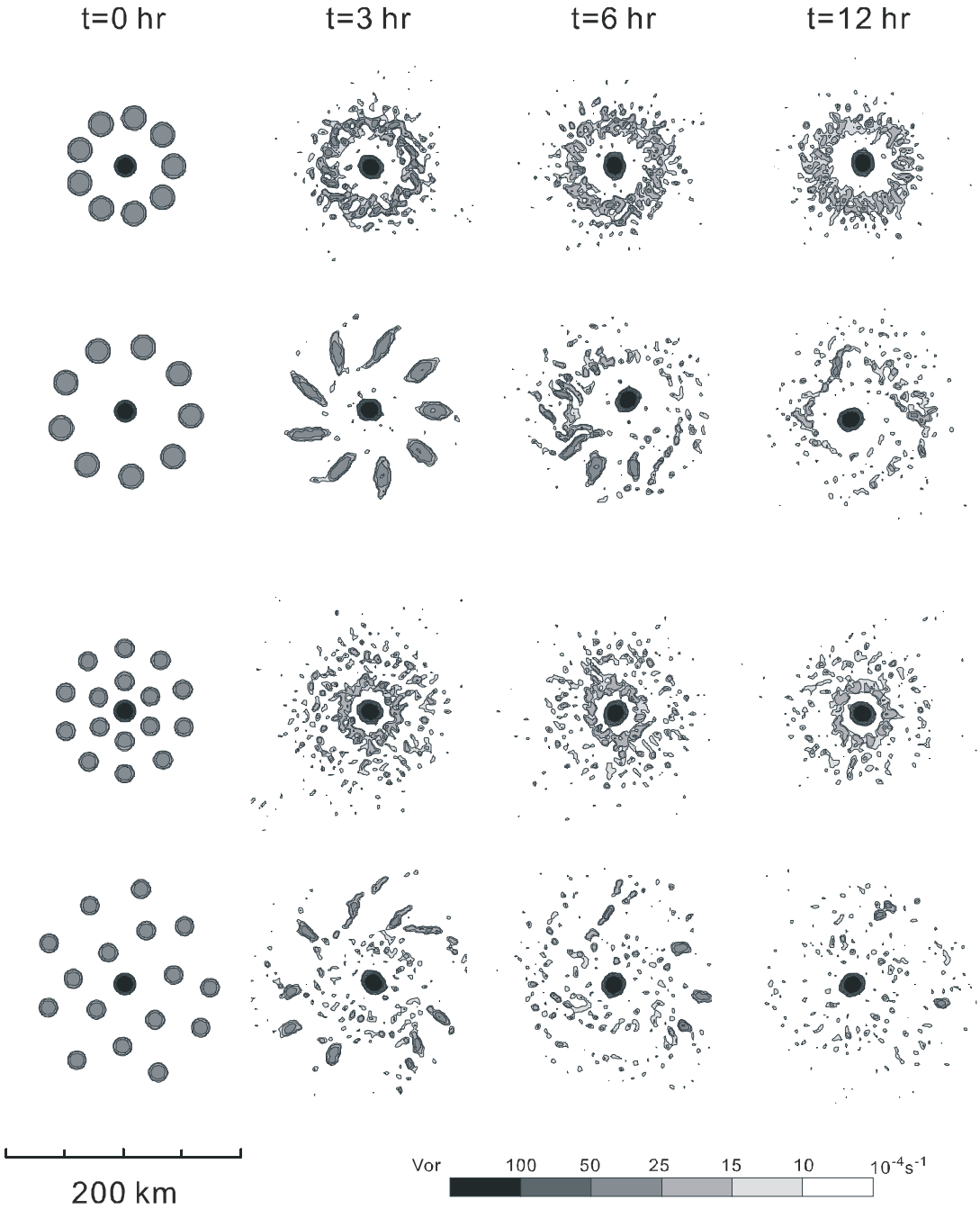

Figure 12: The multiple vortex experiments with nine and sixteen neighboring vortices. The total neighboring vorticity is the same as in the benchmark binary vortex experiments.

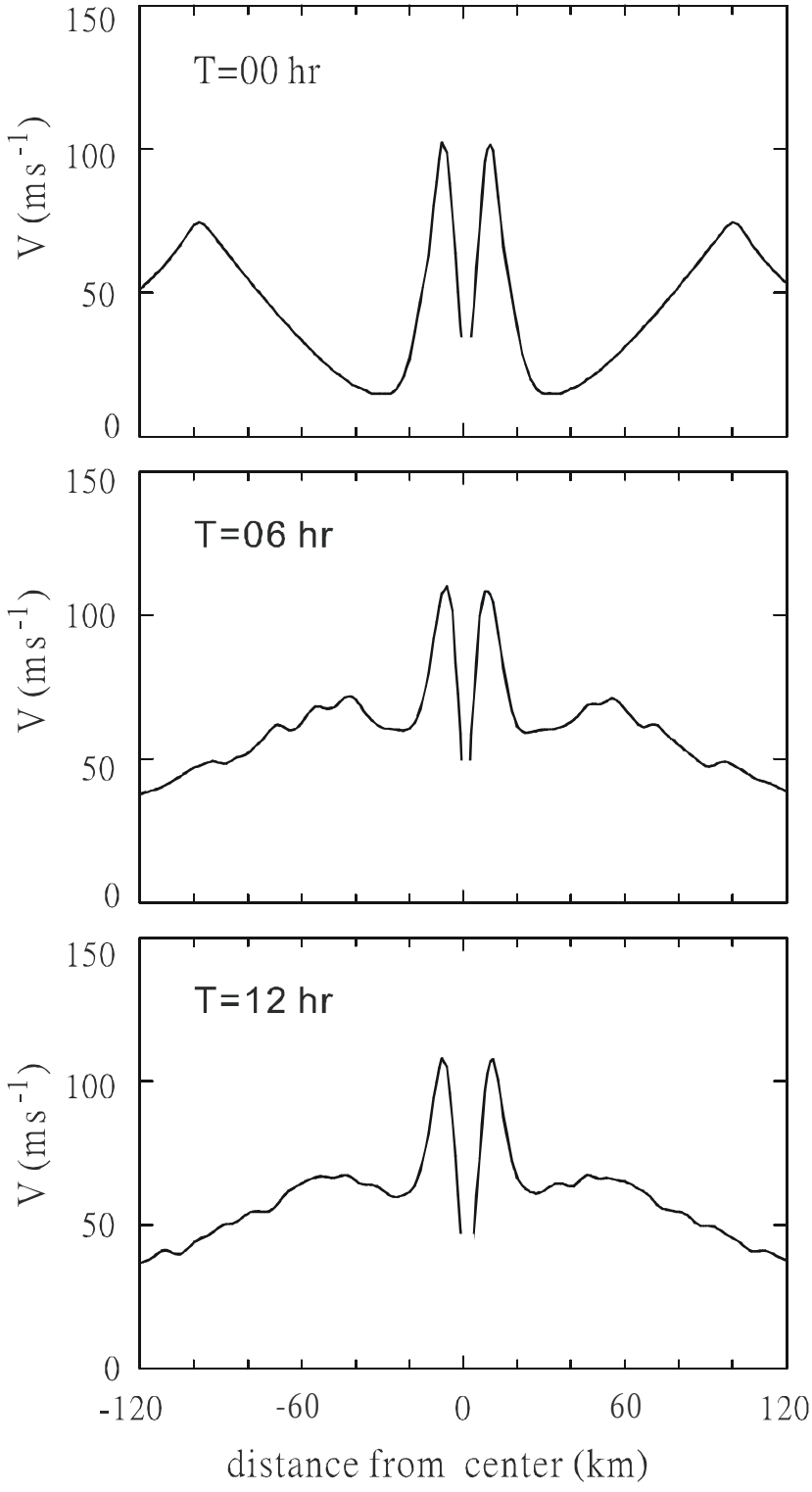

Figure 13: The tangential wind speed for radial arms toward the west (left portion) and the south (right portion) that emanate from the vortex center at various times for the experiment in the second row of Figure11.

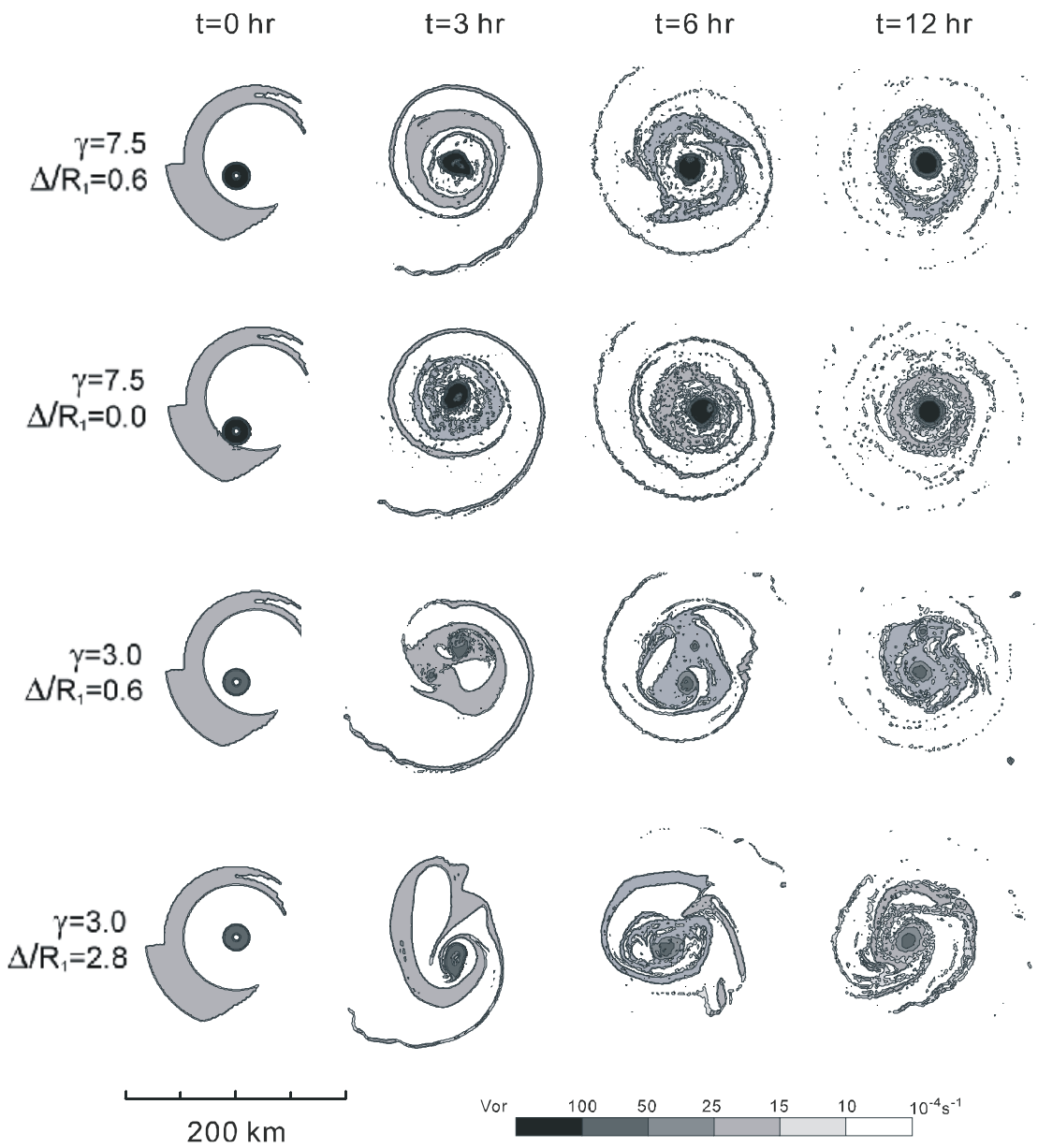

Figure 14: The Lekima experiments with a core vortex and an area of weak vortivity that resembles of the shape of convection as observed in the radar picture. The control experiment on the top row has the vorticity strength ratio γ=7.5 and the shortest distance from the outer vorticity boundary to the core vortex boundary is Δ/R_1=0.6 (R_1=10 km). The parameter in second row is the same with the control except with the parameter Δ/R_1=0. The parameters in the third row is the same as the control except with γ=3. The parameters in the bottom row are Δ/R_1=2.8 and γ=3.